

Research paper

Design, synthesis and characterization of dual inhibitors against new targets FabG4 and HtdX of *Mycobacterium tuberculosis*Deb Ranjan Banerjee^a, Rupam Biswas^b, Amit K. Das^{b,*}, Amit Basak^{a,c,**}^a Department of Chemistry, Indian Institute of Technology, Kharagpur 721302, India^b Department of Biotechnology, Indian Institute of Technology, Kharagpur 721302, India^c School of Bioscience, Indian Institute of Technology, Kharagpur 721302, India

ARTICLE INFO

Article history:

Received 1 February 2015

Received in revised form

21 May 2015

Accepted 3 June 2015

Available online 6 June 2015

Keywords:

Tuberculosis

FabG4

HtdX

MIC

Biofilm

Polypharmacology

ABSTRACT

Herein, we present dual inhibitors of new targets FabG4 and HtdX for the first time. In this work, eight compounds have been designed, synthesized, characterized and evaluated for bio-activities. Amongst them, six compounds have shown inhibitory activities. Three of them (**12–14**) demonstrate dual inhibition of both FabG4 and HtdX at low micromolar concentration. In addition, the dual inhibitors show good anti-mycobacterial properties against both planktonic growth and biofilm culture of *Mycobacterium* species. This study is an important addition to tuberculosis drug discovery because it explores two new enzymes as drug targets and presents their dual inhibitors as good candidates for pre-clinical trials.

© 2015 Elsevier Masson SAS. All rights reserved.

1. Introduction

Tuberculosis (TB) still remains as one of the major infectious diseases worldwide; approximately one third of global population is infected by its causative agent, *Mycobacterium tuberculosis* (*Mtb*) and 1.3 million died from the disease in 2012 [1]. Due to emergence of multi drug resistant (MDR) and extremely drug resistant (XDR) *Mtb* strains, a numbers of first line TB drugs such as isoniazid, rifampicin, pyraniazid, ethambutol and streptomycin have failed in recent TB cases [2]. Besides, treatment of tuberculosis is a long-time procedure that requires almost 6–9 months of multiple antibiotic therapies to avoid the re-emergence of the disease [3]. The reason behind this long treatment procedure is biofilm-like pellicle growth by *Mtb* which is distinct from planktonic growth [4]. The pellicle shows increased phenotypic resistance and harbors drug-resistant *Mtb* cells which persist despite exposure of high concentrations of antibiotics. In this persistent stage, *Mtb* remains in slow growing or non-growing state and leads to the asymptomatic latent infection.

Thus, the combined effects of both genetic and phenotypic resistance by *Mtb* is forcing the scientific community to come up with new drug targets and alternate drugs which are crucial to stop this ancient pathogen from further killing.

Mtb possesses lipid rich cell wall, produced by fatty acid synthesis (FAS) pathway, required for its survival within host cell. *Mtb* cells become virtually impenetrable to the antibiotics due to presence of the thick lipid rich envelop. FAS pathway not only required in planktonic growth but also implicated in the formation of pellicle during the latent infection [5]. The FAS generally consists of two different pathways, namely FAS-I and FAS-II [6]. FAS-I is a multi-domain enzyme, involved in the *de novo* synthesis of short chain fatty acids. FAS-II is involved in the production of very long chain fatty acids and composed of discrete mono-functional enzymes. Apart from FAS I and FAS II, many bypass fatty acid biosynthetic pathways are possibly present in *Mtb* and these have been implicated to its drug resistance behavior [7–9]. Besides, the inherent redundancy of polygenic *Mtb* network makes it impossible to shut down a cellular pathway by taking out a single target. Thus, the enzymes involved in bypass pathways provide attractive targets for alternate anti-TB drug discovery. Our targets FabG4 (Rv0242c) and HtdX (Rv0241c) are two such less explored enzymes that belong to a single fatty acid metabolizing operon of *Mtb* (Fig. 1). This operon is

* Corresponding author.

** Corresponding author. Department of Chemistry, Indian Institute of Technology, Kharagpur 721302, India.

E-mail addresses: amitk@hijli.iitkgp.ernet.in (A.K. Das), absk@chem.iitkgp.ernet.in (A. Basak).

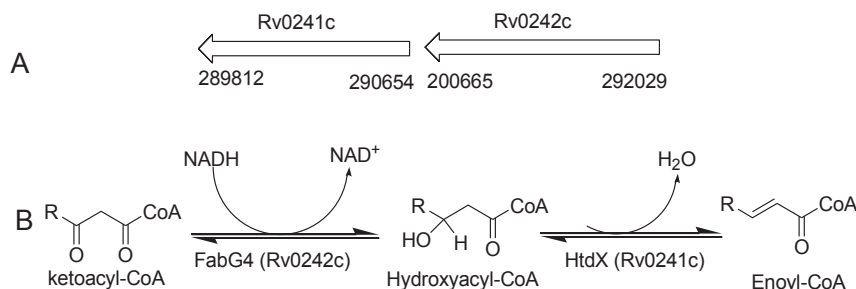


Fig. 1. A. The genomic arrangement of Rv0242c (FabG4) and Rv0241c (HtdX) in conserved putative fatty acid metabolizing operon (OperonDB, confidence = 84, n = 57); B. Basic functions of FabG4 and HtdX; FabG4 and HtdX are involved in two consecutive steps of fatty acid metabolism.

conserved among most actinobacteria and some lipid rich proteobacteria and might be involved in interlinked [8] CoA dependent fatty acid metabolism pathway [10] instead of traditional FAS pathway. The FabG4, a β -ketoacyl CoA reductase, is recently reported to be an essential and functional protein for bacterial growth, survival [11] and fatty acid synthesis [12]. There are five *fabG* genes present in *Mtb* genome [13], but only *fabG1* (rv1483) and *fabG4* (rv0242c) are conserved among mycobacterial species. FabG4 is possibly involved in genetic resistance of *Mtb* as it is over-expressed in sub-inhibitory concentrations of streptomycin [14]. It is also linked with pellicle formation as it is over-expressed in biofilm mode of growth [15]. Thus, it is a potential target for alternative drugs that can be administered with frontline TB drugs to shorten the TB treatment time. The other enzyme of interest is HtdX (Rv0241c), a 3(R)-hydroxyacyl CoA dehydratase, is also a member of the conserved operon. The enzyme functions in a dehydration step after reduction of ketoacyl substrate by FabG4 (Fig. 1). Alike FabG4, HtdX is also a physiologically functional and essential for the bacillus growth and fatty acid production [16]. The enzyme is hypothesized to be involved in bypass fatty acid synthesis pathway and in drug resistance of *Mtb* [8,10c,17,18]. There are eleven putative (R)-specific hydratase/dehydratase candidates identified in *Mtb*, but only HadB (Rv0636) and HtdX are – (i) ubiquitous among every mycobacteria and related mycolate-producing genera; (ii) contain characteristic and well conserved catalytic sequence, called ‘hydratase 2 motif’ [19]. *In vitro* activity of purified HtdX has been checked and it has shown 3-hydroxyacyl dehydratase/*trans*-2-enoyl hydratase activity with preference for CoA as carrier unit of the acyl chain [10c]. Also, HtdX and FabG4 can plausibly function within a shared pathway as they both belong to single operon [16,18,20]. This type of pair arrangement has been observed in other enzymes of FAS family, including FabG1 (Rv1483) and InhA (Rv1484) [6]. These reports and facts have made HtdX a potential target for the drug discovery along with FabG4. Recently, the crystal structures of FabG4 [20] and HtdX [18] have been solved which build up the platform to design structure-based inhibitors against the enzymes concerned.

As FabG4 and HtdX are involved in consecutive steps of fatty acid metabolism and plausibly function within a shared interlinked pathway, a single inhibitor that can inhibit both FabG4 and HtdX may result in synergistic effect in overall therapeutic efficacy. Moreover, a single drug that can simultaneously interact with multiple targets (polypharmacology) [21] is found to be more efficient against advance-stage polygenic pathologies [22] compared to a combination drugs with high specificity for a different targets. Combination of drugs (combination therapy) has several drawbacks like drug–drug interaction, increased toxicities compared to a single drug with multi-target efficiencies [23]. Additionally, multi-target single therapeutic agent has more

predictable pharmacokinetic and pharmacodynamic properties and less adverse effect due to administration of a single drug [23]. Inspired by these prospects, we undertook the task to develop dual inhibitors of both FabG4 and HtdX for the first time. The strategy to design dual inhibitors through blending of structure-based and ligand-based design is described. These designed hybrids have been synthesized, characterized and evaluated for their bioactivities. Inhibition profiles have been analyzed by various biophysical methods (inhibition kinetics, ITC, CD) and molecular docking study. In addition, growth inhibition assays of these novel dual inhibitors has been checked against both planktonic and biofilm growth of *Mycobacterium*.

2. Results and discussion

2.1. Design concept for dual inhibitor

Rational design of multi-targeting inhibitor remained as a challenging task for a medicinal chemist, particularly for a combination of structurally divergent targets, namely FabG4 and HtdX for the present case. A good design strategy determines the difference between ‘targeted polypharmacology’ and ‘drug promiscuity’ [23]. Considering this scenario, the number of articles containing rational designing of drugs with desired multi-target profiles has increased steadily in recent times. One such design strategy adopts combination of common pharmacophore selection and molecular docking study [24]. For our case, we adopt a 3-steps design strategy that combines both structure-based and ligand-based designing.

2.1.1. Step 1: target site analysis of FabG4 and HtdX

The crystal structure of FabG4 with co-factor NADH and substrate Hexanoyl CoA (PDB ID: 3V1U) shows that the active site of FabG4 could be accessed from two different sides: a narrow minor portal and a wide major portal. The co-factor NADH binds at the relatively wide major portal, while thinner fatty acyl substrate accesses the active site *via* minor portal (Fig. 2) [25]. For NAD-dependent enzyme like FabG4 where substrate binding site (minor portal) is narrow and intrinsically non-druggable, NAD binding pocket (major portal) can be a viable drug target [26]. The NAD binding site can be divided into three subsites, the nicotinamide binding subsite (N-subsite), the adenosine binding subsite (A-subsite) and the pyrophosphate binding subsite (P-subsite). If a ligand binds at all or any of these subsites, it will selectively repel NAD and thus should act as an inhibitor of the enzyme. Based on these structural insights, we targeted NAD binding pocket for inhibitor designing against FabG4. In addition, the active site of FabG4 is composed catalytic tetrad Ser347, Tyr360, Lys364 and Asn319. The active site is covered by two catalytic loops, namely loop-I and loop-II. Movement of these catalytic loops is crucial

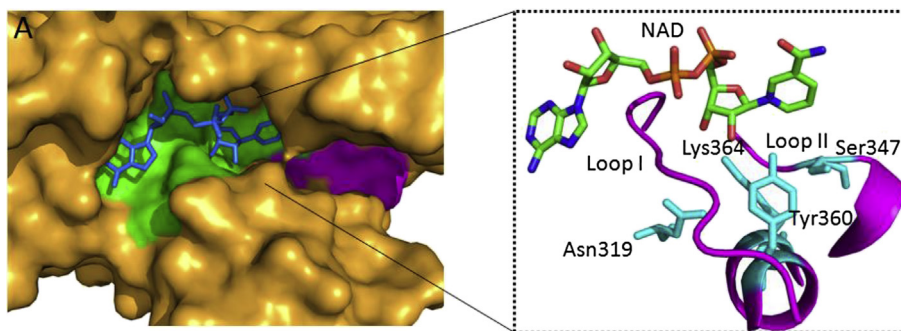


Fig. 2. NADH bound FabG4 structure with close view of catalytic tetrad (Asn319, Ser347, Tyr360, Lys364) and catalytic loops (I and II). NADH binds at wide major portal (green), minor portal (magenta) is narrow. (For interpretation of the references to color in this figure caption, the reader is referred to the web version of this article.)

during the enzymatic action of FabG4. Loop I consists of a conserved NAG triad (Asn295, Ala296, Gly297) which interacts with pyrophosphate part of the NADH and directs the cofactor towards active site.

The crystal structure of HtdX (PDB ID: 3WEW) shows that it has a characteristic double hot dog fold (DHD) motif [18]. Alignment of amino acid sequence of HtdX with *M. tuberculosis* HadB, eukaryotic peroxisomal dehydrogenase and hydratase 2 has shown that the catalytic loop of HtdX consists of 26 amino acids (Gly161–Gly185) (Fig. 3). In this catalytic loop, active site residues Asp162 and His167 provide the conserved basic hydratase 2 motif consisting of [Asp]-x(4)-His sequence [19]. Couple of glycines at both terminals of the catalytic loop governs the flexibility for the binding of variable hydrophobic tails of substrates. In addition, the active site cavity is covered by hydrophobic lid comprising Ile171, Leu175, Phe176 and Phe178 (Fig. 3). The inner cavity of catalytic tunnel is negatively charged and acidic. Therefore, a ligand can inhibit the HtdX by occupying the hydrophobic entrance and plugging the hydrophilic catalytic tunnel *via* interacting with the active site residues. Based on these structural insights, we targeted catalytic loop of HtdX for inhibitor designing.

2.1.2. Step 2: selection of common pharmacophores

Based on structural knowledge of the target sites, we chose pharmacophores from ligand-based screening. For the enzymatic action of both FabG4 and HtdX, movements of the loops (loop I-loop II of FabG4 and catalytic loop of HtdX) are essential. To restrict the loop movements, we chose conformationally constrained β -lactam moiety as a common pharmacophore in our design. Besides, the carbonyl group at C-2 of β -lactam ring can interact with the protein residues and delivers the rigidity to the binding site. Isoniazid (INH) was chosen as another pharmacophore based on following rationale: Isoniazid is a bio-isostere of nicotinamide ring due to structural and chemical similarity between the two. Hence, Isoniazid is a potential N-subsite binder of NADH binding site and a natural pharmacophore of FabG4. Again, HtdX catalytic tunnel is negatively charged and acidic; while Isoniazid is basic and partially positively charged. Hence, Isoniazid is a potential binder at the catalytic tunnel of HtdX due to favorable charge interaction. Besides, Zhang et al. have reported [27] nicotinic hydrazide (isomer of isoniazid) linked Schiff bases as competitive inhibitor of another dehydratase enzyme (*HpFabZ*) involved in bacterial FAS II. In addition, aromatic rings were also chosen as common pharmacophores in order to interact with the hydrophobic lid of HtdX catalytic loop.

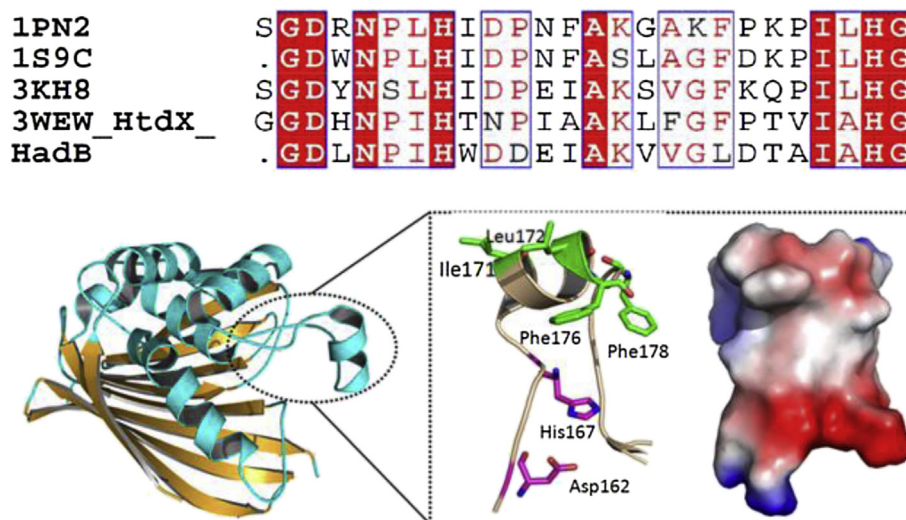


Fig. 3. (At top) Alignment of amino acid sequence of the catalytic loop of *M. tuberculosis* HtdX (3WEW) with *C. tropicalis* 2-Enoyl-CoA hydratase 2 (1PN2), peroxisomal dehydrogenase/hydratase 2 (1S9C), *P. capsici* Mao-C like dehydratase (3KH8) and *M. tuberculosis* HadB. Red boxes indicate highly conserved residues; (at below) Overall structure of HtdX with close view of catalytic loop. Active site residues Asp162 and His167 are inside the active site tunnel, the outer hydrophobic lid consists of Ile171, Leu175, Phe176 and Phe178. Vacuum electrostatics contact potential of catalytic loop (from the same face) shows that the deep of catalytic tunnel is highly negative charged (red). (For interpretation of the references to color in this figure caption, the reader is referred to the web version of this article.)

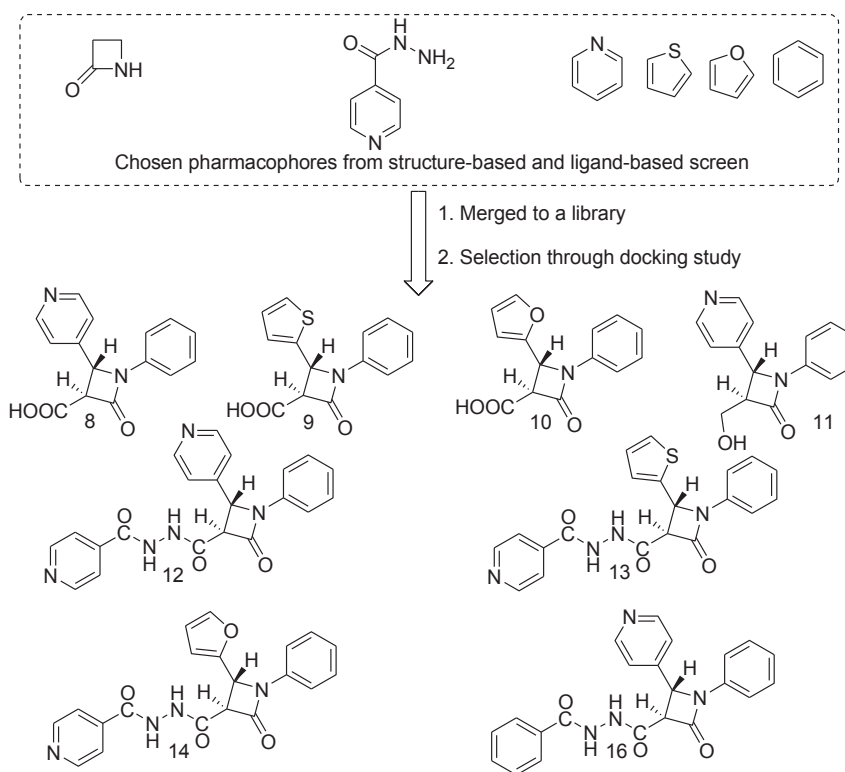


Fig. 4. Eight designed compounds as possible inhibitors of FabG4 and HtdX.

2.1.3. Step 3: In silico selection

After selecting the common pharmacophores for both the targets, we merged them to obtain a small library. From the library, final candidates were selected using stepwise docking studies. Following this procedure, we designed seven compounds (**8–14**, Fig. 4) as candidates for later parts of this work. Amongst them, compounds **12–14**, that contain Isoniazid as a fragment of their structure, showed most promising docking results against both FabG4 and HtdX. Additionally, compound **16** was designed through replacing Isoniazid fragment of compound **12** by non-polar benzhydrazide fragment.

2.2. Chemistry

The methodology to obtain the designed compounds is shown in Scheme 1 and 2. The key step to obtain the designed compounds was Kinugasa reaction [28] involving cycloaddition between various nitrones and *in situ* generated copper acetylide from ethyl propiolate which provided the β -lactam core. In this synthesis procedure, no protecting group was necessary that reduced the number of steps and increased the overall yield.

The various nitrones employed as the partner for Kinugasa reaction were prepared starting from the phenyl hydroxylamine which was reacted with various aldehydes (4-pyridinecarboxaldehyde/2-thiophenecarboxaldehyde/2-furan carboxaldehyde) in dry methanol that led to the desired nitrones (**2,3,4**). The Kinugasa reactions were performed in between the respective nitrone and ethyl propiolate in presence of CuI (1 eq) in dry DMF to obtain β -lactam esters (**5,6,7**). The esters were hydrolysed carefully at low temperature using 0.1 N LiOH in methanol-water (1:1) solvent to obtain corresponding β -lactam acids (**8,9,10**) (Scheme 1). Additionally, compound **11** was synthesized *via* reduction of compound **8** with sodium borohydride in methanol.

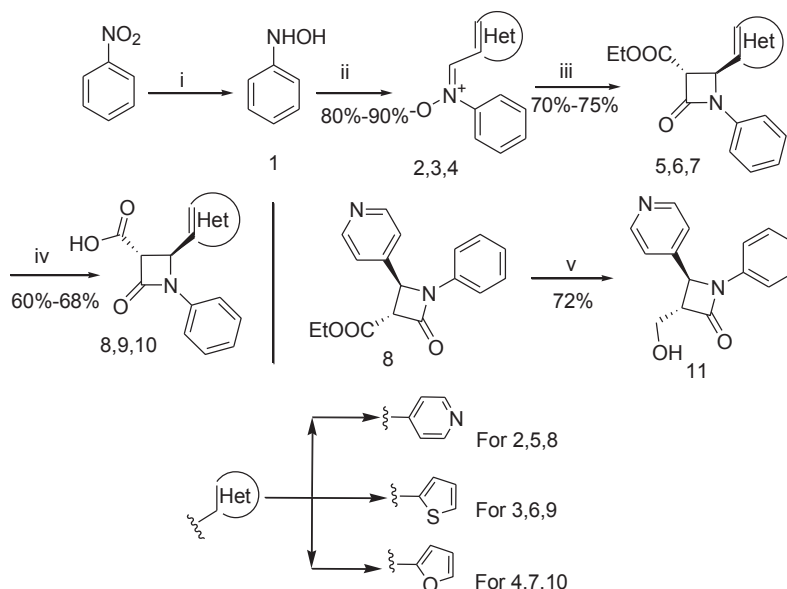
Subsequent treatment of β -lactam acids produced rest of designed compounds as depicted in Scheme 2. Isoniazid linked compounds (**12–14**) were synthesized by EDC-mediated coupling of β -lactam acids (**8–10**) with Isoniazid. For the synthesis of compound **16**, benzhydrazide (**15**) was prepared from benzoic acid *via* chlorination followed by coupling with hydrazine hydrate. Subsequent EDC-mediated coupling with β -lactam acid **8** furnished compound **16**.

All final compounds were characterized by ^1H , ^{13}C NMR and mass spectra. Purity of these compounds was checked through reverse-phase analytical HPLC (selective traces are given in SI). Finally, structure of one Isoniazid linked derivative was confirmed through X-ray crystal structure determination of **14** (ORTEP shown in Fig. 5).

2.3. Inhibition kinetics

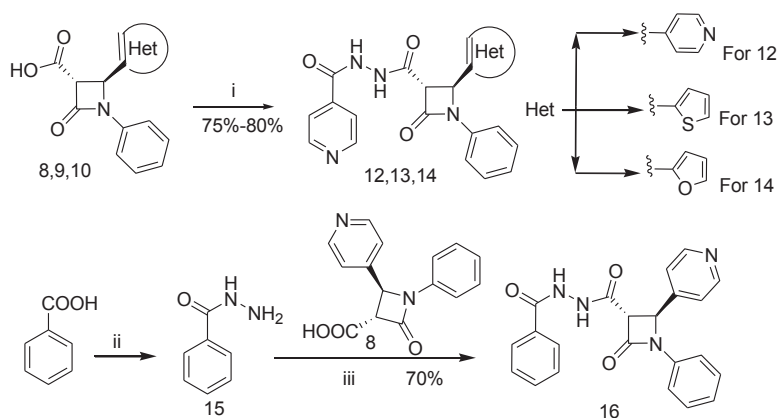
2.3.1. Inhibition of FabG4

Inhibition kinetics of compounds **8–14** and **16** was carried out against FabG4 at 25 °C by monitoring the decrease in absorbance at 340 nm due to the conversion of NADH to NAD^+ . Half maximal inhibitory concentration (IC_{50}) values were evaluated by varying inhibitor concentrations until full inhibition occurred. Amongst the β -lactam acids (**8,9,10**), only compound **8** that contains pyridyl substituent at C-4 of β -lactam ring, inhibits the enzyme at micromolar concentration ($\text{IC}_{50} = 64.3 \pm 1 \mu\text{M}$). This result shows that pyridyl substituent has significant influence on FabG4 inhibition as compared to thiophenyl/furyl substituent and corroborates with the fact that NADH binding pocket is a good target of pyridine nucleus containing natural product like pyridomycin [29]. Moreover, NADH is itself a highly polar compound and its binding pocket naturally prefers polar substituent like pyridine ring than hydrophobic substituent like thiophene or furan ring. Docking study of compound **8** with FabG4 indicates that pyridine ring binds near the N-site, whereas the adjacent carboxyl acid group interacts with



Reagents and conditions: i) Zn dust, NH_4Cl , H_2O (s), 50°C , 15 min; ii) Respective aldehydes, methanol (s), 12 h; iii) Ethyl propiolate, CuI , Et_3N , DMF (s), 24 h; iv) 0.1 N LiOH , methanol (s), 20°C , 6 h; v) NaBH_4 , Methanol (s), 30 min

Scheme 1. General synthetic scheme for the synthesis of designed β -lactam compounds.



Reagents and conditions: i) Isoniazid, EDC-Cl, HOBT, DMAP, dry DCM (s), 16 h ii) SOCl_2 , $\text{N}_2\text{H}_4\cdot\text{H}_2\text{O}$, 10 min, 0°C ; iii) EDC-Cl, Et_3N , HOBT, DCM (s), 12 h

Scheme 2. Synthesis of designed hybrid compounds.

nearby active site residue. Inhibition kinetics of compound **11** that contains pyridyl substituent at same position was used to cross-check the finding. Compound **11** also inhibits FabG4, but the inhibitory power is minimum ($\text{IC}_{50} = 666.1 \pm 20 \mu\text{M}$); that may be

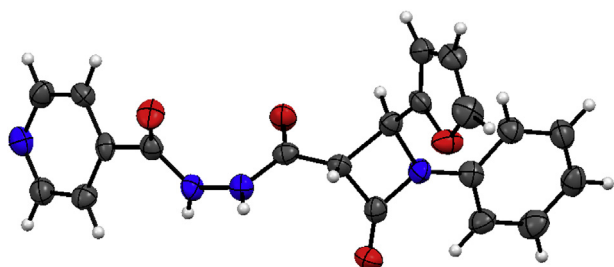
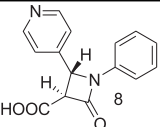
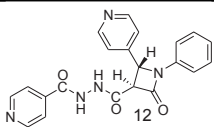
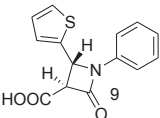
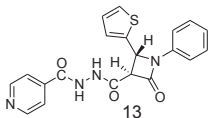
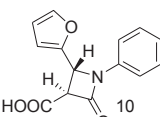
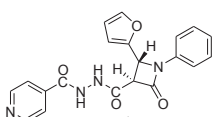
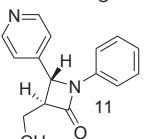
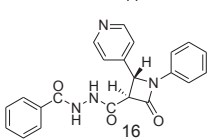


Fig. 5. ORTEP image of **14** (CCDC number 1042896).

due to the replacement of carboxylic acid group of **8** by alcohol moiety adjacent to pyridyl ring.

All Isoniazid linked hybrids (**12,13,14**) with most promising docking results inhibited FabG4 at low micro molar concentrations. Amongst them, hybrid **12** that contains pyridine substituent attached to β -lactam ring showed highest inhibition ($\text{IC}_{50} = 15.2 \pm 0.5 \mu\text{M}$) of FabG4 enzyme. Although, thiophene and furan containing β -lactam acids (**9,10**) could not inhibit FabG4 up to 1 mM concentration, but their isoniazid coupled products (**13, 14**) inhibited FabG4 enzyme at low micromolar concentrations. Above result validates our designing strategy that Isoniazid fragment plays a crucial role in binding of these compounds at NADH binding pocket. Moreover, the benzhydrazide linked compound (**16**) exhibited approximately three times less inhibitory potency ($\text{IC}_{50} = 39.9 \pm 2 \mu\text{M}$) than its Isoniazid bound analogue (**12**) and that further elucidates the practical implication of Isoniazid in FabG4

Table 1
Inhibition profiles of designed and synthesized compounds.

Compound	IC ₅₀ against <i>Mtb</i> -FabG4 (in μ M)	IC ₅₀ against <i>Mtb</i> -HtdX (in μ M)	Compound	IC ₅₀ against <i>Mtb</i> -FabG4 (in μ M)	IC ₅₀ against <i>Mtb</i> -HtdX (in μ M)
	64.3 \pm 1	No inhibition		15.2 \pm 0.5	22.3 \pm 0.5
	No inhibition	No inhibition		26.1 \pm 1.5	10.3 \pm 0.8
	No inhibition	No inhibition		27.6 \pm 1	17.6 \pm 0.9
	666.1 \pm 20	No inhibition		39.9 \pm 2	No inhibition

inhibition. Mode of inhibition of the best found inhibitor (**12**) was evaluated against FabG4 with varying NADH concentration at three different concentrations of inhibitor. The compound **12** was found to be competitive with respect to NADH. Competitive inhibition also substantiates with designing that these inhibitors target NADH binding site.

2.3.2. Inhibition of HtdX

The enzyme assay of HtdX was performed spectrophotometrically (at 263 nm) in presence of crotonoyl-CoA as substrate [10c]. Inhibition kinetics of compounds **8–14** and **16** were carried out to screen their inhibition potencies. The β -lactam acids (**8,9,10**) and compound **11** were found to be inactive against HtdX up to 1 mM concentration. But Isoniazid linked compounds (**12,13,14**) demonstrated strong HtdX inhibition at low micromolar concentrations. The hybrid **13** with aromatic thiophene substituent at C-4 of β -lactam ring showed best inhibition (IC₅₀ = 10.3 \pm 0.8 μ M) of HtdX; whereas the hybrid compound **12** with polar pyridine substituent at the same end showed somewhat less inhibition (IC₅₀ = 22.3 \pm 0.5 μ M). This inhibitory tendencies verifies our design strategy that aromatic substituent linked to β -lactam ring assist the inhibitor to bind at catalytic loop *via* hydrophobic aromatic interaction with the hydrophobic lid at the entrance of the loop. The benzhydrazone linked compound (**16**), the analogue of compound **12** with benzhydrazone fragment in place of isoniazid fragment, could not inhibit HtdX up to 1 mM concentration. The inability of compound **16** to inhibit HtdX strongly demonstrates the significance of isoniazid fragment in HtdX inhibition and indicates polar interactions with the isoniazid fragment with the hydrophilic catalytic tunnel residues is the main driving force behind the inhibitor binding. Additionally, mode of inhibition of the best found inhibitor (**13**) was checked with varying crotonoyl-CoA concentration at three different concentrations of inhibitor. Compound **13** is found to be competitive with respect to crotonoyl-CoA. This competitive mode of inhibition supports our claim that the designed inhibitors bind at the catalytic loop and prevent the fatty acyl substrate to enter in to the catalytic tunnel.

2.3.3. Dual inhibition of FabG4 and HtdX

From the listed *in vitro* inhibition profiles of all designed and synthesized compounds against FabG4 and HtdX (Table 1), it can be clearly seen that this study successfully leads to the identification of three novel compounds (**12,13,14**) as potent dual inhibitors of FabG4 and HtdX with IC₅₀ values in low micromolar range. Amongst them, compound **12** showed best inhibition of FabG4; while compound **13** was found as best inhibitor of HtdX.

2.4. Isothermal titration calorimetry (Itc)

2.4.1. FabG4 titration

Isothermal titration calorimetry (ITC) of FabG4 with the best found inhibitor (compound **12**) was performed at 25 °C to obtain the thermodynamic parameters of binding. To understand the binding nature of compound **12**, FabG4-**12** titration was compared with FabG4-NADH titration (as NADH was used as a substrate in inhibition kinetics). FabG4 exists as an inseparable homo-dimer in solution and two NADH molecules bind sequentially to each monomer with negative co-operativity [30]. Thus, NADH binding to first monomer is co-operative to NADH binding to second monomer and the co-operativity effect carries through dimeric interface [31]. The binding curve of FabG4-**12** titration fits well to the 'sequential binding' mode with number of binding site (N = 2). Bindings of compound **12** with both the monomers of FabG4 dimer are spontaneous as indicated by negative ΔG values (Table 2). Moreover, negative ΔH and ΔS values signify enthalpically favored bindings and interactions *via* good hydrogen bonding and conformational changes. The first binding constant ($K_1 = 2.98 \times 10^5 \text{ M}^{-1}$) is higher than second binding constant ($K_2 = 1.15 \times 10^3 \text{ M}^{-1}$) which indicates negative co-operativity. Thus, calorimetry of compound **12** with FabG4 reveals that it also binds sequentially to each monomer of FabG4 dimer with negative co-operativity as followed in case of NADH. Therefore, this similarity in binding nature of FabG4-NADH binding and FabG4-**12** binding with a distinct trend of negative cooperativity at two sites of FabG4 dimer supports that designed inhibitors binds at the NADH binding pocket of FabG4.

Table 2Mode of bindings, binding constants and thermodynamic parameters from FabG4-**12** and HtdX-**13** titrations.

Titration	Mode of binding	Binding constant K (Mol ⁻¹)	Thermodynamic parameters		
			ΔH (Kcal/Mol)	ΔS (Cal/Mol/K)	ΔG (Kcal/Mol)
FabG4- 12	Sequential binding with number of binding sites (N) = 2	$K_1 = 2.98 \times 10^5$ $K_2 = 1.15 \times 10^3$	$\Delta H_1 = -15.7$ $\Delta H_2 = -4.8 \times 10^2$	$\Delta S_1 = -27.8$ $\Delta S_2 = -1.6 \times 10^3$	$\Delta G_1 = -7.4$ $\Delta G_2 = -4.0$
HtdX- 13	One site binding	$K = 4.21 \times 10^5$	$\Delta H = -66.2$	$\Delta S = -196$	$\Delta G = -7.8$

Table 3The changes in secondary structures of FabG4 and HtdX on interaction with **12** and **13** respectively.

	FabG4	FabG4-12 (1:5)	HtdX	HtdX-13 (1:5)
Helix (%)	25.9	30	12.2	11.1
β -sheet (%)	6.0	5.7	40.1	50.6
Turns (%)	34.6	29.8	12.6	2.6
Unorderd (%)	33.5	34.4	35.2	35.7

2.4.2. HtdX titration

ITC was used to evaluate the parameters of binding between HtdX and its best found inhibitor (compound **13**). HtdX-**13** titration was carried out at 25 °C. The integrated binding isotherm fits to the 'one site' binding model with number of binding site (N) close to one. The binding of compound **13** with HtdX is spontaneous (negative ΔG) with high binding constant ($K = 4.21 \times 10^5 \text{ M}^{-1}$) (Table 2). The overall binding process is enthalpically favoured (negative ΔH) that indicates the polar interaction dominates in binding. The negative ΔH along with negative ΔS value indicates interactions via hydrogen bonding and conformational changes which support our design concept.

2.5. Circular dichroism (CD)

Circular dichroism (CD) was conducted to evaluate the change in secondary structures of proteins on binding of these dual inhibitors. For this, CD studies were carried out between FabG4 and **12**, and HtdX and **13** in Jasco-815 automatic spectropolarimeter at 25 °C. In both cases, the molar concentration ratio was 1:5 (protein:ligand) in the micromolar range. Ligands were taken in reaction buffer (Tris) and used for baseline correction followed by two separate runs; one is only protein and another is protein-ligand mixture. The CD spectra of free proteins and their complexes are shown in supporting information. The changes in secondary structures of FabG4 and HtdX on interaction with **12** and **13** were analyzed and given in Table 3.

The percentage of α -helix of FabG4 increases on interaction with **12**. The helicity enhancement is related with co-operativity [32]

and the change in secondary structure supports our previous finding from ITC that FabG4-**12** binding is cooperative in nature. In case of HtdX, helicity and turns slightly decrease, and percentage of beta sheet increases on interaction with **13**.

2.6. Molecular docking study

Molecular docking studies were carried out as a part of design strategy. Here, docking results of FabG4-**12** and HtdX-**13** are described in details. Results of additional docking studies are included in supporting information.

Isoniazid linked compound **12**, best found inhibitor against FabG4, binds at the major portal of FabG4 and blocks all three subsites (A-, P-, N-) of NADH binding site. Moreover, the Isoniazid fragment is directed towards the N-subsite and interacts with catalytic residues Tyr360 via hydrogen bonding interaction and with Lys364 via cation- π interaction. The β -lactam ring along with bis-amide linker binds loop I (P-subsite) and interacts with crucial Gly297 residue via hydrogen bonding interactions. The A-subsite of NADH binding site has been occupied by the aromatic substituent linked to β -lactam ring. In between them, the pyridine substituent makes hydrogen bond with Asp244 and the phenyl substituent experiences a sigma- π type interaction with Ala296 of loop I (Fig. 6A).

Isoniazid linked compound **13**, the best found inhibitor against HtdX, binds at the catalytic loop of HtdX. The aromatic substituent linked to β -lactam ring interacts with the hydrophobic outer lid; while the isoniazid fragment directs towards the inner side of catalytic tunnel. The phenyl and thiophene substituents at 1- and 4-position of lactam ring interact with Phe178 via hydrophobic aromatic interactions. The carboxy group at 3-position of lactam ring makes hydrogen bond with terminal Gly185, a crucial residue for the flexibility and right conformation of the catalytic loop. Finally, the isoniazid fragment interacts with catalytic residue His167 via hydrogen bond formation and with Asp162 via charge interactions (Fig. 6B).

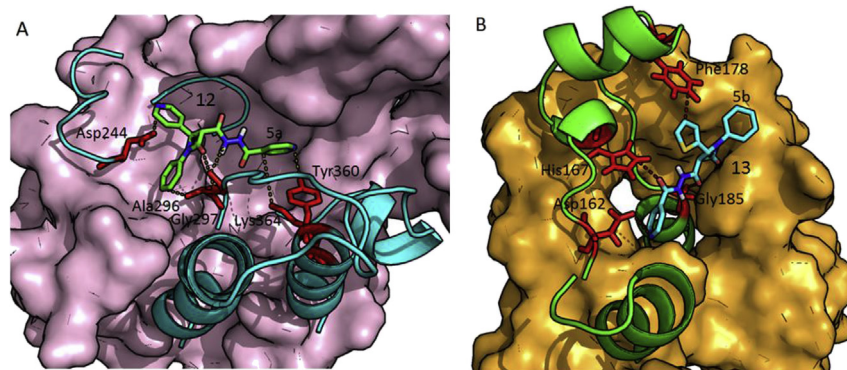


Fig. 6. A. FabG4-**12** docking results: compound **12** binds at major portal of FabG4 and interacts with Tyr360 (catalytic residue), Lys364 (catalytic residue), Gly297, Ala296, Asp244; B. HtdX-**13** docking results: compound **13** binds near catalytic loop and interacts with Gly185, Phe178, His167 (catalytic residue) and Asp162 (catalytic residue). More images are included in supporting information.

2.7. Minimum inhibitory concentration (mic assay)

Anti-mycobacterial activity of the found dual inhibitors was evaluated against *Mycobacterium smegmatis* using aerobic resazurin microplate reduction assay (REMA) [33]. The *M. smegmatis* is non-pathogenic, fast growing and contains both *fabG4* and *htdX* genes in its genomic sequence with high degree of conservations [15,19]. For these reasons, *M. smegmatis* mc²155 strain was chosen as a model organism for this study. The assay conditions were standardized using different concentrations of inoculum, resazurin indicator and reference compound isoniazid (INH). Concentrations of dual inhibitor **12**, **13** and **14** were screened in the range of 0 $\mu\text{g mL}^{-1}$ to 100 $\mu\text{g mL}^{-1}$. Dual inhibitors of FabG4 and HtdX has shown good anti-mycobacterial activities with MIC value 15 $\mu\text{g mL}^{-1}$ (for **12**), 20 $\mu\text{g mL}^{-1}$ (for **13**) and 15 $\mu\text{g mL}^{-1}$ (for **14**), whereas the MIC of reference compound Isoniazid is found to be 10 $\mu\text{g mL}^{-1}$ (REMA plate image is included in [supporting information](#)).

It may be mentioned that MIC of synthesized compounds is probably not due to free Isoniazid liberated through breaking of amide bond (at C-3 of β -lactam) in cellular condition. Because, amide bond at C-3 of β -lactam ring is generally considered as stable in cellular condition as many commercial β -lactam antibiotics (such as Penicillin G, Amoxicillin etc.) contain amide linker at same position in their structures. Amongst them, Amoxicillin is reported to be functional inside mycobacterial cell [34]. Also, the monocyclic β -lactam rings are more stable than bicyclic β -lactam rings [35] and they are least prone to nucleophilic ring opening when no electron withdrawing group is attached to N-1. To crosscheck this possibility, we separately incubated the dual inhibitor **12** in culture media in presence of *M. smegmatis* for 24 h after which, the culture was lyophilized, dissolved in solvent and subjected to HPLC. No trace of Isoniazid was seen in HPLC (traces are included in SI). Above data supports that anti-mycobacterial activity of synthesized dual inhibitors is due to the activity of intact compound and not due to any release of isoniazid during incubation. .

2.8. Biofilm inhibition assay

As already mentioned FabG4 is over-expressed during biofilm formation and linked to latent infection. It is also probable that FabG4 and HtdX, members of same operon, function through interlinked pathway. Hence, we have screened the synthesized dual inhibitors of FabG4-HtdX pair against biofilm formation by *Mycobacterium* species. Again, non-pathogenic *M. smegmatis* has been chosen as model organism as it contains both *fabg4* and *htdX* genes in its genome sequence [15,19]. Besides, biofilm formation in *M. smegmatis* is well characterized. [4,5,36] Compound **12** was chosen for this study and its MIC against biofilm formation was determined. It showed complete inhibition of biofilm formation at concentration of 20 $\mu\text{g mL}^{-1}$ (plate image is included in SI). The result is interesting in view of reported resistance of *M. smegmatis* biofilm culture against Isoniazid [36].

3. Conclusion

This is the first report of dual inhibitors against FabG4 and HtdX. Possible involvements of FabG4 and HtdX in bypass fatty acid synthesis pathway, drug resistance and latent infection have implicated them as alternative targets in anti-tuberculosis research due to the unavailability of drugs that can act against drug resistant *Mtb* strain or latent stage tuberculosis. Hence, the dual inhibitor of FabG4 and HtdX has immense potential to be used in pre-clinical trials. In addition, polypharmacology of these dual inhibitors may also results in therapeutic synergy *in vivo* as both FabG4 and HtdX

enzymes belong to single operon and involve in successive steps of fatty acid metabolizing procedure. The dual inhibitors have been designed, synthesized, characterized and evaluated for bio-activities. These hybrids inhibit FabG4 and HtdX at low micromolar concentration and show good anti-mycobacterial property against both planktonic growth and biofilm culture. Thus, this study successfully explores FabG4 and HtdX as new anti-TB targets and presents their dual inhibitors as possible lead compounds against the resistant/dormant mycobacterial strain.

4. Experimental section

4.1. Molecular docking

Advanced and widely used molecular grid-based docking program Autodock4.2 was used for molecular docking studies. The X-ray crystal coordinates of FabG4 (PDB ID 4FW8) and HtdX (PDB ID 3WEW) were obtained from the Protein Data Bank (<http://www.rcsb.org>). Prior to dockings, receptor structures were edited by adding hydrogen atoms and gasteiger charges in autodocktools to create PDBQT files. Crucial residues at probable binding sites of receptors were selected as flexible residues to perform flexible dockings. Ligand PDB structures were built up using Accelrys Discovery studio 3.1 client. Energy minimization of ligand structures were carried out using CHARMM force field. Ligand PDB files were edited in autodocktools by defining root center, aromatic carbons, torsions and saved as PDBQT files. In grid selections, the whole receptor structures were selected for autogrid calculation with 0.375 Å spacing to perform blind dockings. Finally, docking studies were carried out using Lamarckian genetic algorithm based on the grid maps of all atoms present in the receptors and ligands. Parameters were used with an initial population of 150 randomly placed individuals, a maximum of 2.5×10^7 energy evaluations, cluster tolerance of 2 Å (rms), output level 1 and maximum of 2.7×10^4 numbers of generations. After each docking execution, the docked conformers were analyzed by autodocktools, pymol and discovery studio 3.1 client. The images were made using pymol viewing software.

4.2. Chemical synthesis and analysis

All common reagents were commercial grade reagents and used without further purification unless necessary. All reactions were conducted with oven-dried glassware under an atmosphere of argon (Ar) or nitrogen (N₂). The solvents were dried by standard methods and purified by distillation before use. Silica gel (60–120 and 230–400 mesh) and alumina (neutral and basic) were used for column chromatography. TLC was performed on aluminum-backed plates and UV-lamp chamber or I₂-blower was used as the TLC spot indicator. The NMR spectra were recorded at Bruker 200 MHz and 400 MHz machine. The following abbreviations are used to describe peak patterns where appropriate: s = singlet, d = doublet, t = triplet, q = quartet, m = multiplet, dd = double doublet, ABq = AB quartet.

4.3. General procedure for the synthesis of nitrones (2,3,4)

A solution of the aldehyde (4-pyridine carboxaldehyde/thiophen-2-aldehyde/furfural, 10 mmol) and phenyl hydroxyl amine (10 mmol) in dry methanol (30 mL) was stirred in room temperature for 12 h under argon atmosphere. Upon completion of the reaction as indicated by TLC, the solution was dried under *vacuo* to leave a residue from which pure nitrones were isolated by flash column chromatography (Neutral alumina for **2**, Si-gel for **3**, **4**) using 2:1 PE/EA as eluent. Spectral characteristics of the purified

compounds are mentioned below:

Compound 2: Yield: 80%; State: light yellow solid; mp: 145 °C; δ_{H} (CDCl₃, 200 MHz): 8.75 (2H, d, $J = 7.1$ Hz), 8.17 (2H, d, $J = 5.4$ Hz), 7.96 (1H, s), 7.74–7.79 (2H, m), 7.49–7.53 (3H, m); δ_{C} (CDCl₃, 50 MHz): 150.5, 136.9, 132.4, 132.4, 130.7, 129.3, 121.7, 121.6.

Compound 3: Yield: 85%; State: light yellow solid; mp: 75 °C; δ_{H} (CDCl₃, 200 MHz): 8.48 (1H, s), 7.75–7.80 (2H, m), 7.37–7.58 (5H, m), 7.14 (1H, m); δ_{C} (CDCl₃, 50 MHz): 146.3, 132.9, 131.2, 130.0, 129.8, 129.1, 129.0, 127.0, 120.9.

Compound 4: Yield: 89%; State: light yellow solid; mp: 78 °C; δ_{H} (CDCl₃, 400 MHz): 8.17 (1H, s), 8.02 (1H, d, $J = 3.6$ Hz), 7.60–7.80 (2H, m), 7.59 (1H, s), 7.45–7.51 (3H, m), 6.65–6.66 (1H, m); δ_{C} (CDCl₃, 50 MHz): 147.6, 144.9, 130.1, 129.4, 124.7, 121.2, 116.9, 112.9, 112.7.

4.4. General procedure of Kinugasa reaction for the synthesis of β -lactams (5,6,7)

To degassed dry DMF (20 mL), ethyl propiolate (500 μ L, 5 mmol), CuI (1.9 g, 10 mmol) and Et₃N (1.4 mL, 10 mmol) were sequentially added and stirred for 30 min at 0 °C. To this mixture, degassed solution of nitrones (**2–4**, 2.5 mmol) in DMF (20 mL) was added and stirred for 24 h at room temperature under argon. The mixture was then poured in water and filtered through celite. The celite bed was thoroughly washed with EtOAc. The combined filtrate was taken in a separatory funnel and the EtOAc layer was repeatedly washed with satd. NH₄Cl and brine and dried over Na₂SO₄. The solvent was removed and the residue upon flash column chromatography (Neutral alumina for **5**, Si-gel for **6**, **7**) using 1:1 PE/EA as eluent afforded the target β -lactams. Spectral characteristics of the purified compounds are mentioned below:

4.5. *Trans* [N-phenyl-3-ethoxycarbonyl-4(4-pyridyl)]-2-azetidinone (**5**)

Yield: 70%; State: red gummy liquid; δ_{H} (CDCl₃, 200 MHz): 8.61–8.58 (2H, d, $J = 6$ Hz), 7.29–7.01 (7H, m), 5.31 (1H, d, $J = 2.6$ Hz), 4.25 (2H, q, $J = 7.1$ Hz), 3.94 (1H, d, $J = 2.6$ Hz), 1.29 (3H, t, $J = 7.2$ Hz); δ_{C} (CDCl₃, 50 MHz): 165.6, 158.4, 150.7, 145.3, 136.6, 129.2, 124.7, 120.9, 116.9, 62.9, 62.4, 56.0, 14.1. HRMS (ES⁺): Calcd. For C₁₇H₁₆N₂O₃ + H⁺ 297.1239, found 297.1344.

4.6. *Trans* [N-phenyl-3-ethoxycarbonyl-4(2-thienyl)]-2-azetidinone (**6**)

Yield: 75%; State: reddish-yellow gummy liquid; δ_{H} (CDCl₃, 200 MHz): 7.37–6.98 (8H, m), 5.62 (1H, d, $J = 2.6$ Hz), 4.30 (2H, q, $J = 7.2$ Hz), 4.14 (1H, d, $J = 2.6$ Hz), 1.33 (3H, t, $J = 7.2$ Hz); δ_{C} (CDCl₃, 50 MHz): 166.0, 159.0, 140.0, 137.0, 129.2, 127.4, 126.8, 126.5, 124.6, 117.3, 64.5, 62.3, 53.6, 14.2. HRMS (ES⁺): Calcd. for C₁₆H₁₅NO₃S + H⁺ 302.0851, found 302.0867.

4.7. *Trans* [N-phenyl-3-ethoxycarbonyl-4(2-furyl)]-2-azetidinone (**7**)

Yield: 73%; State: Yellow gummy liquid; δ_{H} (CDCl₃, 400 MHz): 7.41–7.25 (5H, m), 7.10–7.06 (1H, m), 6.54–6.53 (1H, m), 6.39–6.37 (1H, m), 5.37 (1H, d, $J = 2.8$ Hz), 4.32 (1H, d, $J = 2.4$ Hz), 4.28 (2H, q, $J = 7.2$ Hz), 1.33 (3H, t, $J = 7.2$ Hz); δ_{C} (CDCl₃, 100 MHz): 166.2, 159.1, 148.7, 143.7, 137.4, 129.2, 124.6, 117.0, 110.8, 110.7, 62.3, 60.5, 50.9, 14.3. HRMS (ES⁺): Calcd. for C₁₆H₁₅NO₄ + H⁺ 286.1079, found 286.1123.

4.8. General procedure of the ester hydrolysis for the synthesis of **8–10**

To a solution of ester (**5–7**, 0.5 mmol) in methanol (20 mL) at 0 °C, 0.1 N LiOH (5 mL) was slowly added and the mixture was stirred at 20 °C for 6 h. It was then carefully acidified using 0.5 N HCl at ice-cold condition. The mixture was partitioned between EtOAc and water (50 mL each). The aqueous layer was back extracted with EtOAc (3 x 50 mL). Combined organic layers were dried over Na₂SO₄ and evaporated under reduced pressure to produce the target compounds which were purified by repeated precipitation from EtOAc-hexane. Spectral characteristics of the purified compounds are mentioned below:

4.9. *Trans* [N-phenyl-4(4-pyridyl)]-2-azetidinone-3-carboxylic acid (**8**)

Yield: 60%; State: red sticky mass; δ_{H} (Acetone-d₆, 400 MHz): 8.63 (2H, m, Ar-H), 7.50 (2H, d, $J = 4.4$ Hz, Ar-H), 7.35–7.27 (4H, m, Ar-H), 7.12–7.10 (1H, m, Ar-H), 5.45 (1H, d, $J = 2.8$ Hz, H-4), 4.23 (1H, d, $J = 2$ Hz, H-3); δ_{C} (Acetone-d₆, 100 MHz): 167.4, 159.8, 151.0, 147.0, 138.1, 130.0, 125.2, 122.5, 117.7, 63.7, 56.9; HRMS (ES⁺): Calcd. For C₁₅H₁₂N₂O₃ + H⁺ 269.0926, found 269.0948.

4.10. *Trans* [N-phenyl-4(2-thienyl)]-2-azetidinone-3-carboxylic acid (**9**)

Yield: 65%; State: reddish yellow sticky mass; δ_{H} (Acetone-d₆, 400 MHz): 7.45–7.27 (6H, m), 7.08–7.03 (2H, m), 5.74 (1H, bs), 3.67 (1H, bs); δ_{C} (Acetone-d₆, 100 MHz): 170.9, 168.0, 141.6, 138.3, 130.0, 128.3, 128.2, 127.3, 125.1, 117.9, 60.6, 52.4; HRMS (ES⁺): Calcd. For C₁₄H₁₁NO₃S + Na⁺ 296.0357, found 296.0400.

4.11. *Trans* [N-phenyl-4(2-furyl)]-2-azetidinone-3-carboxylic acid (**10**)

Yield: 68%; State: dark yellow sticky mass; δ_{H} (CDCl₃, 400 MHz): 9.03 (1H, bs), 7.40–7.24 (5H, m), 7.10–7.06 (1H, m), 6.55 (1H, d, $J = 2.8$ Hz), 6.37 (1H, q, $J = 2$ Hz), 5.39 (1H, d, $J = 2$ Hz), 4.39 (1H, d, $J = 2.4$ Hz); δ_{C} (CDCl₃, 100 MHz): 170.1, 159.1, 148.1, 143.8, 137.1, 129.2, 124.9, 117.2, 110.9, 110.9, 60.0, 51.1; HRMS (ES⁺): Calcd. For C₁₄H₁₁NO₄ + Na⁺ 258.0766, found 258.0804.

4.12. Synthesis of *trans* [3-(hydroxymethyl)-1-phenyl-4-(4-pyridyl)]-2-azetidinone (**11**)

To a solution of **8** (70 mg, 0.24 mmol) in methanol (10 mL), NaBH₄ (19 mg, 0.5 mmol) was added pinch-wise and stirred for 30 min at room temperature. After completion of the reaction as indicated by TLC, the reaction mixture was quenched with satd. NH₄Cl solution and extracted with EtOAc. The organic layer was washed by brine, dried over Na₂SO₄ and evaporated under reduced pressure. The residue upon flash column chromatography (neutral alumina, 2:1 PE-EA as eluent) afforded the pure compounds. Spectral characteristics of the purified compounds are mentioned below:

Yield: 72%; State: red sticky mass; δ_{H} (CDCl₃, 400 MHz): 8.62 (2H, bs), 7.32–7.24 (6H, m), 7.11–7.07 (1H, m), 5.06 (1H, d, $J = 2.4$ Hz), 4.18 (1H, dd, $J = 12$ Hz, 4.8 Hz), 4.05 (1H, dd, $J = 12$ Hz, 4 Hz), 3.37 (1H, t, $J = 5.2$ Hz), 3.28 (1H, bs); δ_{C} (CDCl₃, 100 MHz): 164.9, 150.5, 147.3, 137.1, 129.4, 124.6, 121.1, 117.0, 62.2, 58.7, 56.2; HRMS (ES⁺): Calcd. For C₁₅H₁₄N₂O₂ + H⁺ 255.1134, found 255.1106.

4.13. General procedure of EDC coupling reaction for the synthesis of 12–14

In dry DCM (10 mL), compound **8–10** (0.2 mmol), EDC-Cl (26 mg, 0.2 mmol), HOBT (27 mg, 0.2 mmol) were added and stirred at 0 °C for 15 min. Isoniazid (23.3 mg, 0.17 mmol) and DMAP (24 mg, 0.2 mmol) were then added and the mixture was stirred at room temperature for 16 h. The mixture was then partitioned between water and DCM (50 mL each) and washed with brine. The organic layer was dried with Na₂SO₄ and evaporated under reduced pressure to leave a residue from which the target compounds were purified by flash column chromatography (neutral alumina) using 10:1 DCM-methanol as eluent. Spectral characteristics of the purified compounds are mentioned below:

4.14. *Trans* [*N'*-isonicotinoyl-2-oxo-1-phenyl-4-(4-pyridyl)]-azetidine-3-carbohydrazide (12)

Yield: 75%; State: reddish sticky mass; δ_H (Acetone-d₆, 400 MHz): 8.77 (2H, d, *J* = 5.6 Hz), 8.64 (2H, d, *J* = 4.6 Hz), 7.82 (2H, d, *J* = 6 Hz), 7.50 (2H, d, *J* = 5.6 Hz), 7.33–7.31 (4H, m), 7.13–7.09 (1H, m), 5.47 (1H, d, *J* = 2.4 Hz), 4.26 (1H, d, *J* = 2.4 Hz); δ_C (Acetone-d₆, 100 MHz): 164.8, 164.8, 160.7, 151.4, 151.3, 146.8, 140.4, 138.1, 130.1, 125.2, 122.2, 122.0, 117.7, 63.0, 56.8; HRMS (ES⁺): Calcd. For C₂₁H₁₇N₅O₃ + H⁺ 388.1410, found 388.1417.

4.15. *Trans* [*N'*-isonicotinoyl-2-oxo-1-phenyl-4-(2-thienyl)]-azetidine-3-carbohydrazide (13)

Yield: 80%; State: reddish-yellow sticky mass; δ_H (CDCl₃, 400 MHz): 8.62 (2H, d, *J* = 4.4 Hz), 7.62 (2H, d, *J* = 5.2 Hz), 7.27–6.92 (8H, m), 5.75 (1H, d, *J* = 1.6 Hz), 4.36 (1H, d, *J* = 2.4 Hz); δ_C (CDCl₃, 100 MHz): 163.6, 163.2, 160.8, 150.4, 139.4, 138.6, 136.6, 129.2, 127.5, 127.4, 126.7, 125.1, 121.4, 117.5, 63.0, 53.4; HRMS (ES⁺): Calcd. For C₂₀H₁₆N₄O₃S + H⁺ 393.1021, found 393.1018.

4.16. *Trans* [*N'*-isonicotinoyl-2-oxo-1-phenyl-4-(2-furyl)]-azetidine-3-carbohydrazide (14)

Yield: 79%; State: reddish-yellow sticky mass; δ_H (Acetonitrile-d₃, 400 MHz): 8.57 (2H, d, *J* = 4.4 Hz), 7.52 (2H, d, *J* = 6 Hz), 7.37 (1H, s), 7.22–7.14 (4H, m), 6.98–6.94 (1H, m), 6.56 (1H, d, *J* = 3.2 Hz), 6.31–6.29 (1H, m), 5.30 (1H, d, *J* = 3.2 Hz), 4.29 (1H, d, *J* = 2.4 Hz); δ_C (Acetonitrile-d₃, 100 MHz): 165.2, 165.2, 161.1, 151.4, 149.5, 144.9, 140.1, 138.0, 130.1, 125.5, 122.1, 117.7, 112.1, 111.8, 59.9, 51.4; HRMS (ES⁺): Calcd. For C₂₀H₁₆N₄O₄ + H⁺ 377.1250, found 377.1251.

4.17. Synthesis of *trans* [*N'*-benzoyl-2-oxo-1-phenyl-4-(4-pyridyl)]-azetidine-3-carbohydrazide (16)

To a solution of compound **8** (0.2 mmol) in dry DCM, HOBT (27 mg, 0.2 mmol) and EDC-Cl (26 mg, 0.2 mmol) were added and stirred for 15 min at 0 °C. Benzhydrazide (**7**, 0.2 mmol) and Et₃N (20 μ L, 0.2 mmol) were then added and stirred for 12 h at room temperature. It was then partitioned between DCM and water, the organic layer was washed with brine. The organic layer was dried over Na₂SO₄ and evaporated at reduced pressure. The residue upon flash column chromatography (Si-gel, 10:1 DCM-methanol as eluent) furnished the target compounds. Spectral characteristics of the purified compounds are mentioned below:

Yield: 70%; State: red-yellow sticky mass; δ_H (Acetone-d₆, 400 MHz): 8.64 (2H, d, *J* = 4.4 Hz), 7.98 (2H, d, *J* = 7.6 Hz), 7.61–7.49 (5H, m), 7.32–7.31 (4H, m), 7.10 (1H, m), 5.51 (1H, d, *J* = 2.4 Hz), 4.17 (1H, d, *J* = 2.8 Hz); δ_C (Acetone-d₆, 100 MHz): 167.3, 167.0, 159.9, 151.0, 147.1, 138.1, 133.9, 132.7, 130.1, 129.3, 128.3, 125.2, 122.5, 117.7,

63.6, 56.9; HRMS (ES⁺): Calcd. For C₂₂H₁₈N₄O₃ + H⁺ 387.1457, found 387.1507.

4.18. Protein purification and inhibition kinetics

4.18.1. FabG4 purification and inhibition kinetics

Detailed procedure of protein purification had been described elsewhere [20]. The inhibition studies were carried out by measuring the decrease of OD340 nm due to the conversion of NADH to NAD⁺ in Evolution™ 300 UV–Visible spectrophotometer (Thermo Fisher scientific) at 25 °C. The assay was done in HEPES buffer (50 mM, pH = 7.4) in a volume of 500 μ L. The acetoacetyl-CoA and β -NADH were purchased from sigma and dissolved in miliQ water to desired stocks concentrations. The inhibitor compounds were dissolved in HPLC grade methanol to a primary stock of 10 mM concentration. From that various diluted stocks were prepared using methanol and exactly 25 μ L of inhibitor solution was added to 500 μ L reaction mixture to maintain the same percentage of methanol (5%) in every assay. This 5% methanol was also added to the controls to nullify the effect of methanol on inhibition kinetics. The typical reaction mixture contained 25 μ L of inhibitor solution in methanol, 0.5 mM acetoacetyl-CoA, 0.2 mM β -NADH, 1 μ M of FabG4 and remaining HEPES buffer in the final volume of 500 μ L. A mixture of 25 μ L inhibitor in methanol, 0.5 mM acetoacetyl-CoA and 1 μ M FabG4 in 500 μ L buffer was used for baseline correction (negative control) before each assay; while mixture of 25 μ L methanol (without inhibitor), 0.5 mM acetoacetyl-CoA, 1 μ M FabG4 and 0.2 mM β -NADH in 500 μ L buffer was used as positive control. The reaction was initiated by the addition of acetoacetyl-CoA. The decrease in absorbance was recorded in every 2 min interval. IC₅₀ values were determined by varying inhibitor concentrations until full inhibition occurred. Enzyme activities were measured with varying NADH concentrations at three different concentrations of inhibitor to determine the mode of inhibition. The IC₅₀ values were calculated graphically from dose–response plots. Modes of inhibition were determined from Lineweaver–Burk plots.

4.18.2. HtdX purification and inhibition kinetics

The details of HtdX purification has been described previously from this group [18]. Inhibition kinetics were performed spectrophotometrically at 263 nm by using crotonoyl-CoA as substrate in Evolution™ 300 UV–Visible spectrophotometer at 25 °C. The assays were done in HEPES buffer (50 mM, pH = 7.5) in presence of 100 mM NaCl with a final volume of 500 μ L. The crotonoyl-CoA was purchased from sigma and dissolved in miliQ water to desired stock concentration. The inhibitor solutions were prepared as described in FabG4 inhibition kinetics section and similarly 25 μ L of inhibitor solution was added to 500 μ L reaction mixture to maintain the same percentage of methanol (5%) in every assay. This 5% methanol was also added to the controls to nullify the effect of methanol on inhibition kinetics. The typical reaction mixture contained 25 μ L of inhibitor solution in methanol, 10 μ M crotonoyl-CoA, 100 nM HtdX and remaining buffer in the final volume of 500 μ L. A mixture of 25 μ L inhibitor in methanol and 100 nM HtdX in 500 μ L buffer was used for baseline correction (negative control) before each assay; while mixture of 25 μ L methanol (without inhibitor), 10 μ M crotonoyl-CoA and 100 nM HtdX in 500 μ L buffer was used as positive control. The reaction was initiated by the addition of crotonoyl-CoA. The decrease in absorbance was recorded in every 2 min interval. IC₅₀ values were determined by varying inhibitor concentrations until full inhibition occurred. Mode of inhibition was measured by varying crotonoyl-CoA concentrations at three different concentrations of inhibitor. The IC₅₀ values were calculated graphically from dose–response plots. Modes of inhibition

were determined from Lineweaver–Burk plots.

4.19. Methods of ITC study

FabG4-**12** and HtdX-**13** ITC studies were carried out in Microcal ITC₂₀₀ instrument at 25 °C. Reference power of 5 μ cal/s, stirring speed of 500 rpm, duration of each injection 0.8 s, filter period 5 s with 120 s spacing were selected as parameters for these studies. FabG4 stock solution was prepared in 50 mM HEPES buffer (pH 7.4); while HtdX solution was prepared in HEPES buffer (50 mM, pH = 7.5) in presence of 100 mM NaCl. Compound stock solutions were prepared in 5% methanol-respective buffers. This extra methanol was also added to the sample cell to avoid large heat change due to solvent mismatch (Getting Started, MicroCal ITC200). All stock solutions were degasified properly before performing experiments. Finally, 4.5 μ M FabG4 solution was taken in sample cell and titrated with 500 μ M compound **12** solution. Similarly, 10 μ M HtdX solution (in sample cell) was titrated against 500 μ M compound **13** solution. Separate buffer-ligand titrations were carried out in each case as reference runs by taking buffer in the sample cell. These reference values were subtracted from the protein-ligand titrations to nullify heat of dissolution. One injection of 0.4 μ L followed by nineteen injections of 2 μ L of ligand solutions were titrated into protein solutions in both cases. The data were solved using MicroCal, LLC ITC 200 software.

4.20. Methods of CD study

CD measurements were carried out on a Jasco-815 automatic recording spectrophotometer, using a path length of 10 mm at 25 °C. The spectra were recorded in the range of 195–240 nm with a scan rate of 50 nm/min and a response time of 1 s. For baseline correction, CD spectra of buffer (10 mM tris buffer of pH 6.8) containing 50 μ M ligands were collected and were subtracted from each sample spectra. The CD spectra of protein-ligand complexes were collected at protein to ligand molar ratio 1:5. The ligand concentrations were maintained at 50 μ M with the protein concentration at 10 μ M. Secondary structures analysis were carried out using DICHROWEB [37], an online server for protein secondary structure analysis from CD spectroscopic data.

4.21. Methods of MIC assay

M. smegmatis mc²155 strain was grown in Middlebrook 7H9 broth with 0.2% glycerol and 0.05% Tween 80 for 20 h at 37 °C with shaking at 120 rpm till the cells reached mid-logarithmic phase (OD₅₉₅ ~ 0.5). Reference compound isoniazid (INH) was dissolved in distilled water to primary stock solution (5 mg/mL) and serially diluted in MB 7H9 media to working stock solution (0.5 mg/mL). All synthesized inhibitors were dissolved in DMSO to an initial stock of 5 mg/mL and two fold diluted in MB 7H9 media to working stock solution (0.5 mg/mL). Resazurin sodium salt was purchased from Sisco Research Laboratories, India. 0.5% (w/v) stock solution of resazurin was prepared in distilled water, filter sterilized and diluted to 0.02% in distilled water.

The inoculum was omitted from row A (negative control), only 50 μ L of media were added to each well. Inhibitor and isoniazid were omitted from row B (growth control), 50 μ L media and 50 μ L of diluted culture (OD₅₉₅ = 0.0005) were added to each well. The media, reference compound isoniazid (INH) and culture were added in row C (positive control). In rows D–F, compound **12**, **13** and **14** were added instead of INH along with culture and media. The total volume in each well was 100 μ L. After 24 h of post-drug incubation at 37 °C, 30 μ L of 0.02% resazurin solution was added to each well and incubated again for 40 min at 37 °C. Color change

from blue (resazurin) to pink (resorufin) indicated the growth of bacteria. The lowest concentrations of drugs which prevented such color change were recorded as MIC. The assay was repeated twice and average of both the experiments was calculated to find the MIC values.

4.22. Methods of biofilm assay

Biofilm of *M. smegmatis* mc²155 was grown in 6-well flat bottomed plate by inoculating 30 μ L (1%) of planktonic culture (growth of *M. smegmatis* planktonic culture already described in previous method) in 3 mL Sauton's minimal media (without Tween-80). Well 1 was used as negative control without any inhibitor, while we added inhibitor **12** at increasing concentration of 5, 10, 20, 50 and 100 μ g mL⁻¹ respectively in well 2 to well 6. The plate was sealed with grease, wrapped up by parafilm and incubated at 37 °C without shaking for 4 weeks. Biofilm formation was easily detected using naked eye. The lowest concentration of inhibitor that prevented biofilm formation was recorded.

Acknowledgment

DRB and AB thank the Council of Scientific and Industrial Research (CSIR) for the fellowship and fund (02(0014)/11/EMR-II). Central Research Facility and Department of Chemistry, IIT Kharagpur are thanked for providing all of the instrumental facilities. AB and AKD gratefully acknowledge the support of DBT for providing the necessary research grant (BT/PR14496/MED/30/550/2010). AB and AKD also acknowledge IIT Kharagpur for SGBSI grant (IIT/SRIC/BIO/LDO/2014-15/33). AB is also grateful to DST for the JC Bose National Fellowship.

Appendix A. Supplementary data

Supplementary data related to this article can be found at <http://dx.doi.org/10.1016/j.ejmech.2015.06.007>.

References

- [1] World Health Organization, Global Tuberculosis Control, 2013. http://www.who.int/tb/publications/global_report/en/.
- [2] (a) S.H.E. Kaufmann, E. Rubin, Handbook of Tuberculosis: Clinics, Diagnostics, Therapy and Epidemiology, Wiley-VCH, 2008, pp. XXIII–XXVII; (b) M.A. Espinal, The global situation of MDR-TB, Tuberculosis 83 (2003) 44–51; (c) C. Lienhardt, M. Raviglione, M. Spigelman, R. Hafner, E. Jaramillo, M. Hoelscher, A. Zumla, J. Gheuens, New drugs for the treatment of tuberculosis: needs, challenges, promise, and prospects for the future, J. Infect. Dis. 205 (2012) S241–S249; (d) C.E. Barry 3rd, J.S. Blanchard, The chemical biology of new drugs in development for tuberculosis, Curr. Opin. Chem. Biol. 14 (2010) 456–466.
- [3] P.C. Hopewell, M. Pai, D. Maher, M. Uplekar, M.C. Raviglione, International standards for tuberculosis care, Lancet Infect. Dis. 6 (2006) 710–725.
- [4] A.K. Ojha, A.D. Baughn, D. Sambandan, T. Hsu, X. Trivelli, Y. Guerardel, A. Alahari, L. Kremer, W.R. Jacobs Jr., G.F. Hatfull, Growth of Mycobacterium tuberculosis biofilms containing free mycolic acids and harbouring drug-tolerant bacteria, Mol. Microbiol. 69 (2008) 164–174.
- [5] A. Ojha, M. Anand, A. Bhatt, L. Kremer, W.R. Jacobs Jr., G.F. Hatfull, GroEL1: a dedicated chaperone involved in mycolic acid biosynthesis during biofilm formation in mycobacteria, Cell 123 (2005) 861–873.
- [6] K. Takayama, C. Wang, G.S. Besra, Pathway to synthesis and processing of mycolic acids in Mycobacterium tuberculosis, Clin. Microb. Rev. 18 (2005) 81–101.
- [7] T. Yoshikawa, D. Norman, Infectious Disease in the Aging: A Clinical Handbook, vol. 46, 2009.
- [8] H.I. Boshoff, T.G. Myers, B.R. Copp, M.R. McNeil, M.A. Wilson, C.E. Barry 3rd, The transcriptional responses of Mycobacterium tuberculosis to inhibitors of metabolism: novel insights into drug mechanisms of action, J. Biol. Chem. 279 (2004) 40174–40184.
- [9] R.J. Kinsella, D.A. Fitzpatrick, C.J. Creevey, J.O. McInerney, Fatty acid biosynthesis in Mycobacterium tuberculosis: lateral gene transfer, adaptive evolution, and gene duplication, PNAS 100 (2003) 10320–10325.
- [10] a) S. Kikuchi, T. Kusaka, z in Mycobacterium smegmatis, J. Biochem. 92 (1982)

- 839–844;
 b) T. Shimakata, Y. Fujita, T. Kusaka, Acetyl-CoA-dependent elongation of fatty acids in *Mycobacterium smegmatis*, *J. Biochem.* 82 (1977) 725–732;
 c) E. Sacco, N. Slama, K. Backbro, T. Parish, F. Laval, M. Daffé, N. Eynard, A. Quemard, Revisiting the assignment of Rv0241c to fatty acid synthase type II of *Mycobacterium tuberculosis*, *J. Bacteriol.* 192 (2010) 4037–4044.
- [11] A. Gurvitz, The essential mycobacterial genes, *fabG1* and *fabG4*, encode 3-oxoacyl-thioester reductases that are functional in yeast mitochondrial fatty acid synthase type 2, *Mol. Genet. Genomics* 282 (2009) 407–416.
- [12] D.J. Beste, M. Espasa, B. Bonde, A.M. Kierzek, G.R. Stewart, J. McFadden, The genetic requirements for fast and slow growth in mycobacteria, *PLoS One* 4 (2009) e5349.
- [13] S.T. Cole, R. Brosch, J. Parkhill, T. Garnier, C. Churcher, D. Harris, S.V. Gordon, K. Eiglmeier, S. Gas, C.E. Barry 3rd, F. Tekai, K. Badcock, D. Basham, D. Brown, T. Chillingworth, R. Connor, R. Davies, K. Devlin, T. Feltham, S. Gentles, N. Hamlin, S. Holroyd, T. Hornsby, K. Jagels, A. Krogh, J. McLean, S. Moule, L. Murphy, K. Oliver, J. Osborne, M.A. Quail, M.A. Rajandream, J. Rogers, S. Rutter, K. Seeger, J. Skelton, R. Squares, S. Squares, J.E. Sulston, K. Taylor, S. Whitehead, B.G. Barrell, Deciphering the biology of *Mycobacterium tuberculosis* from the complete genome sequence, *Nature* 393 (1998) 537–544.
- [14] P. Sharma, B. Kumar, N. Singhal, V.M. Katoch, K. Venkatesan, D.S. Chauhan, D. Bisht, Streptomycin induced protein expression analysis in *Mycobacterium tuberculosis* by two-dimensional gel electrophoresis & mass spectrometry, *Indian J. Med. Res.* 132 (2010) 400–408.
- [15] P.W. Kerns, D.F. Ackhart, R.J. Basaraba, J.G. Leid, M.E. Shirtliff, *Mycobacterium tuberculosis* pellicles express unique proteins recognized by the host humoral response, *Pathog. Dis.* 70 (2014) 347–358.
- [16] A. Gurvitz, J.K. Hiltunen, A.J. Kastaniotis, Heterologous expression of mycobacterial proteins in *Saccharomyces cerevisiae* reveals two physiologically functional 3-hydroxyacyl-thioester dehydratases, *HtdX* and *HtdY*, in addition to *HadABC* and *HtdZ*, *J. Bacteriol.* 191 (2009) 2683–2690.
- [17] S. Kikuchi, T. Kusaka, Purification and crystallization of 3-oxoacyl-CoA synthase of *Mycobacterium tuberculosis*, *J. Biochem.* 94 (1983) 1045–1051.
- [18] R. Biswas, D. Dutta, A.K. Das, Cloning, overexpression, purification, crystallization and preliminary X-ray diffraction analysis of Rv0241c (*HtdX*) from *Mycobacterium tuberculosis* H37Rv, *Acta Cryst.* F69 (2013) 1110–1113.
- [19] E. Sacco, A.S. Covarrubias, H.M. O'Hare, P. Carroll, N. Eynard, T.A. Jones, T. Parish, M. Daffe, K. Backbro, A. Quemard, The missing piece of the type II fatty acid synthase system from *Mycobacterium tuberculosis*, *PNAS* 104 (2007) 14628–14633.
- [20] D. Dutta, S. Bhattacharyya, S. Mukherjee, B. Saha, A.K. Das, Crystal structure of *fabG4* from *Mycobacterium tuberculosis* reveals the importance of C-terminal residues in ketoreductase activity, *J. Struct. Biol.* 174 (2011) 147–155.
- [21] (a) A.L. Hopkins, Network pharmacology: the next paradigm in drug discovery, *Nat. Chem. Biol.* 4 (2008) 682–690;
 (b) A.D.W. Boran, R. Iyengar, Systems approaches to polypharmacology and drug discovery, *Curr. Opin. Drug Discov. Dev.* 13 (2010) 297–309;
 (c) J. Mestres, E. Gregori-Puigjané, Conciliating binding efficiency and polypharmacology, *Trends Pharmacol. Sci.* 30 (2009) 470–474;
 (d) J.U. Peters, Polypharmacology: foe or friend? *J. Med. Chem.* 56 (2013) 8955–8971.
- [22] (a) Z.A. Knight, H. Lin, K.M. Shokat, Targeting the cancer kinome through polypharmacology, *Nat. Rev. Cancer* 10 (2010) 130–137;
 (b) A.C. Dar, T.K. Das, K.M. Shokat, R.L. Cagan, Chemical genetic discovery of targets and anti-targets for Cancer polypharmacology, *Nature* 486 (2012) 80–84;
 (c) A.J.S. Knox, T. Price, M. Pawlak, G. Golfs, C.T. Flood, D. Fayne, D.C. Williams, M.J. Meegan, D.G. Lloyd, Integration of ligand and structure-based virtual screening for the identification of the first dual targeting agent for heat shock protein 90 (*Hsp90*) and tubulin, *J. Med. Chem.* 52 (2009) 2177–2180;
 (d) T.V. Lipina, M. Wang, F. Liu, J.C. Roder, Synergistic interactions between PDE4B and GSK-3: DISC1 mutant mice, *Neuropharmacology* 62 (2012) 1252–1262;
 (e) I. Bolea, J. Juárez-Jiménez, C. De los Ríos, M. Chioua, R. Pouplana, F.J. Luque, M. Unzeta, J. Marco-Contelles, A. Samadi, Synthesis, biological evaluation, and molecular modeling of donepezil and *n*-(5-(benzyloxy)-1-methyl-1H-indol-2-yl)methyl]-*n*-methylprop-2-yn-1-amine hybrids as new multipotent cholinesterase/monoamine oxidase inhibitors for the treatment of Alzheimer's disease, *J. Med. Chem.* 54 (2011) 8251–8270;
 (f) R. Leon, A.G. Garcia, J. Marco-Contelles, Recent advances in the multitarget-directed ligands approach for the treatment of Alzheimer's disease, *Med. Res. Rev.* 33 (2013) 139–189;
 (g) B. Apffel, J.A. Blair, B. Gonzalez, T.M. Nazif, M.E. Feldman, B. Aizenstein, R. Hoffman, R.L. Williams, K.M. Shokat, Z.A. Knight, Targeted polypharmacology: discovery of dual inhibitors of tyrosine and phosphoinositide kinases, *Nat. Chem. Biol.* 4 (2008) 691–699.
- [23] A. Anighoro, J. Bajorath, Rastelli, G. Polypharmacology: challenges and opportunities in drug discovery, *J. Med. Chem.* 57 (2014) 7874–7887.
- [24] D. Wei, X. Jiang, L. Zhou, J. Chen, Z. Chen, C. He, K. Yang, Y. Liu, J. Pei, L. Lai, Discovery of multitarget inhibitors by combining molecular docking with common pharmacophore matching, *J. Med. Chem.* 51 (2008) 7882–7888.
- [25] D. Dutta, S. Bhattacharyya, A. Roychowdhury, R. Biswas, A.K. Das, Crystal structure of Hexanoyl-CoA bound to β -ketoacyl reductase *fabG4* of *Mycobacterium tuberculosis*, *Biochem. J.* 450 (2013) 127–139.
- [26] I. Giangreco, M.J. Packer, Pharmacophore binding motifs for nicotinamide adenine dinucleotide analogues across multiple protein families: a detailed contact-based analysis of the interaction between proteins and NAD(P) co-factors, *J. Med. Chem.* 56 (2013) 6175–6189.
- [27] L. Zhang, W. Liu, T. Hu, L. Du, C. Luo, K. Chen, X. Shen, H. Jiang, Structural basis for catalytic and inhibitory mechanisms of β -Hydroxyacyl-acyl carrier protein dehydratase (*fabZ*), *J. Biol. Chem.* 283 (2008) 5370–5379.
- [28] (a) A. Basak, H.M. Bdour, G. Bhattacharya, *Tetrahedron Lett.* 38 (1997) 2535;
 (b) A. Basak, G. Bhattacharya, H.M.M. Bdour, *Tetrahedron* 54 (1998) 6529;
 (c) A. Basak, S.C. Ghosh, T. Bhowmick, A.K. Das, V. Bertolasi, *Tetrahedron Lett.* 43 (2002) 5499;
 (d) A. Basak, R. Pal, *Bioorg. Med. Chem. Lett.* 15 (2005) 2015;
 (e) A. Basak, K. Chandra, R. Pal, S.C. Ghosh, Kinugasa reaction under click chemistry conditions, *Synlett* (2007) 1585–1588;
 (f) M. Kinugasa, S. Hashimoto, The reactions of copper (I) phenylacetylide with nitrones, *J. Chem. Soc. Chem. Commun.* (1972) 466–467;
 (g) J. Marco-Contelles, β -Lactam synthesis by the Kinugasa reaction, in: *Angew. Chem. Int. (Ed.)* 43, 2004, pp. 2198–2200.
- [29] (a) R.C. Hartkoorn, C. Sala, J. Neres, F. Pojer, S. Magnet, R. Mukherjee, S. Uplekar, S. Boy-Rottger, K.H. Altmann, S.T. Cole, Towards a new tuberculosis drug: pyridomycin: nature's isoniazid, *EMBO Mol. Med.* 4 (2012) 1032–1042.
- [30] D.R. Banerjee, D. Dutta, B. Saha, S. Bhattacharyya, K. Senapati, A.K. Das, A. Basak, Design, synthesis and characterization of novel inhibitors against mycobacterial β -ketoacyl CoA reductase *fabG4*, *Org. Biomol. Chem.* 12 (2014) 73–85.
- [31] D. Dutta, S. Bhattacharyya, A.K. Das, Crystal structure and fluorescence studies reveal the role of helical dimeric interface of staphylococcal *fabG1* in positive cooperativity for NADPH, *Proteins: Struct. Funct. Bioinf* 80 (2012) 1250.
- [32] T. Bereau, M. Deserno, M. Bachmann, Structural basis of folding cooperativity in model proteins: insights from a microcanonical perspective, *Biophys. J.* 100 (2011) 2764–2772.
- [33] J.C. Palomino, A. Martin, M. Camacho, H. Guerra, J. Swings, F. Portaels, Resazurin microtiter assay plate: simple and inexpensive method for detection of drug resistance in *Mycobacterium tuberculosis*, *Antimicrob. Agents Chemother.* 46 (2002) 2720–2722.
- [34] M.H. Cynamon, G.S. Palmer, In vitro activity of amoxicillin in combination with clavulanic acid against *Mycobacterium tuberculosis*, *Antimicrob. Agents Chemother.* 24 (1983) 429–431.
- [35] (a) H. Kojo, Y. Mine, M. Nishida, S. Goto, S. Kuwahara, Nature of monocyclic beta-lactam antibiotic nocardicin A to beta-lactamases, *Microbiol. Immunol.* 32 (1988) 119–130;
 (b) R. Méndez, T. Alemany, J. Martín-Villacorta, Stability in aqueous solution of two monocyclic beta-lactam antibiotics: aztreonam and nocardicin A, *Chem. Pharm. Bull.* 40 (1992) 3222–3227.
- [36] R. Teng, T. Dick, Isoniazid resistance of exponentially growing *Mycobacterium smegmatis* biofilm culture, *FEMS Microbiol. Lett.* 227 (2003) 171–174.
- [37] L. Whitmore, B.A. Wallace, Protein secondary structure analyses from CD spectroscopy, *Biopolymers* 89 (2008) 392–400.